#25-138
2025 AFS Proceedings ©American Foundry Society

Digital Characterization of Casting Surfaces

Daniel W. Schimpf
Volkswagen, Kassel, Hesse, Germany

Frank E. Peters
Iowa State University, Ames, Iowa, USA

ABSTRACT

Casting surface specifications are based on aesthetics, functionality or a combination of both. To classify casting surfaces, visual inspections are performed by an operator who compares the casting surface to images or comparator plates that represent a certain roughness level. This inspection process is highly subjective, disagreements arise on the acceptance of a casting between the casting producer and buyer. To minimize these disagreements and use developments in 3D scanning, the objective of this project is to develop a digital surface characterization method. The method developed and implemented in this project utilizes underlying geometry estimation, abnormality detection, and a new roughness characterization formula based on a variogram to determine a surface roughness value. Tests were done to compare the new roughness characterization formula with existing quantification methods and to compare the results of the method with human operators.

Keywords: casting surface, inspection, comparator plates, digital surface characterization

INTRODUCTION

During the casting design process, the casting surface is assigned a roughness specification. Once the casting is produced, typically a human operator determines if a surface is within specifications by comparing the casting surface with roughness standards. These standards can be images or comparator plates made from plastic or metal. During the inspection process, the inspector tries to determine which comparator plate or image best matches the surface. When using reference images, only the eyesight of the inspector is utilized to compare the surfaces. Some examples of these would be the ACI Surface Indicator Scale[1] and the MSS SP-55 Visual Method.[2] In the case of comparator plates, the inspector also uses his/her vision with the option of using tactile sense to find the best matching reference surface. One of the popular standards in the United States is ASTM A802,[3] which references the plastic comparator plates provided by the Steel Castings Research and Trade Association (SCRATA), Figure 1. The SCRATA comparator plates do not only classify surface roughness but also other surface characteristics such as inclusions, gas porosity, discontinuities (fusion and expansion) or removal marks (thermal, mechanical and welds). Most of these categories have four different levels ranging from smooth to rough, little to many inclusions, or shallow to deep removal marks. One of the disadvantages of the SCRATA plates is the lower resolution with usually only four levels of surface roughness in comparison to the GAR C-9 Cast Microfinish Comparator surface roughness scale, Figure 2, which has nine. The GAR Microfinish Comparator C9 plate states the roughness in the form of Root Mean Square (RMS) from 20 to 900 microinches, but it is not clear how these values were obtained, as the authors have had difficulty replicating these numerical values. This method also does not have any anomaly definitions such as porosity.[4]

Utilizing reference images and comparator plates is subjective because different operators may arrive at different classifications. This may cause problems for producers if the casting buyer's inspector classifies the surface as rougher than the producer inspector. Much research has been done to address visual inspection errors and their causes. One such study[5] was conducted to determine the effectiveness of visual inspection using a visual comparative method, the MSS SP-55. It was found that the effectiveness of inspectors during the final visual inspection of aluminum castings ranged from 69% to 92% with an average of about 82%. The study concluded that with visual standards like the MSS SP-55 effectiveness can only be as high as approximately 80%. A similar study[6] dealt with visual inspection error and its measurement specifically looked at abnormalities on casting surfaces which can also be classified using surface comparison specimen. The Gage Repeatability and Reproducibility (GR&R) study looked at three different foundries with two inspectors and concluded that average reproducibility (within inspector deviation) was 45% matching of results, and the average repeatability (between inspectors) was 64% percent match. Both of these studies show that the classification of surface properties (roughness, abnormalities, etc.) by a human operator is subject to significant error. Another study[7] looked into methods to improve the visual inspection process. The study showed that by training operators the inspection outcome can be improved by using systematic and thorough search patterns (e.g., rastering training)

Figure 1. This is a photo of the SCRATA comparator plates for levels A1 through A4 (left to right)

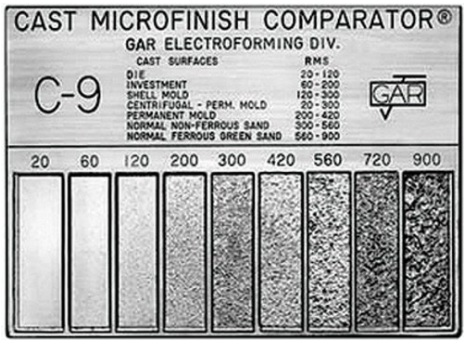

Figure 2. This is a photo of the GAR C-9 Cast Microfinish Comparator surface roughness plate.

One way to improve the reliability of surface roughness characterizations would be to develop an objective digital method to classify casting surfaces. An automated visual inspection process for surface roughness would be problematic as it would need to rely on color or shading information. The inspection would assume that deeper grooves create darker shadows, but these darker shadows would be hard to differentiate from color changes on the surface itself. Thus, two surfaces with the same surface roughness but with one having a color pattern on its surface would likely get different roughness results.

These studies demonstrate the need for an improvement in casting surface characterization. Training human operators to improve their repeatability and reproducibility is not enough, because one will never be able to overcome the subjectivity inherent in the process.

Using 3D methods for measurement purposes is not a new idea. In the machining industry, objective methods to classify surface roughness are widely used. Some of these are contact methods such as a stylus profilometer, but these methods are often time-consuming, limited in their measuring amplitude, mostly line sampling, and may not be able to detect undulations[8,9] which exist on sand castings. Contact methods are widely used on machined surfaces where the surface often has a cyclic character and in general, a lower surface roughness than castings. On the other hand, non-contact methods are able to acquire a large number of three-dimensional surface points in a short time. One popular roughness parameter calculated from 3D data is *Sa* (average roughness) which is essentially the 3D equivalent of the 2D roughness parameter *Ra*. When only one *Ra* profile is compared with the *Sa* parameter for the same surface, differences as high as 52 % have been reported.[10] This difference can be reduced by averaging multiple *Ra* profiles and further reduced by removing profiles parallel to the main feature direction. One disadvantage of currently common areal surface characterization is the small area inspected. The *Sa* parameter, for example, is used in combination with microscopes where the area covered is typically less than 3 by 3 mm.[11] For machined surfaces, this small area may be representable for the whole surface, but this is most often not the case for sand casting surfaces.

Voelker proposed a method for casting characterization that considers the underlying geometry of the surface and possible abnormalities, but spatial information of the points in space was ignored. Voelker utilized a point cloud, which can be acquired with a variety of methods (e.g., time-of-flight, triangulation, structured light), to determine if a surface is as good as a set standard or better. For that, the designer had to define three values: a baseline roughness, an abnormality level, and an abnormality percentage. However, a weakness of this method was the inability to determine a roughness value for a specific surface.[12]

Considering the low reliability of the current visual inspection methods and that current digital methods do not consider spatial relations of 3D data, improvements for the casting surface roughness classification are necessary. The goal of this project is to propose a method that is able to produce reliable and objective surface classifications.

EXPERIMENTAL PROCEDURE

This section will describe the different methods that were developed for the surface characterization as well as the device that was developed for the mobile roughness determination.

SPATIAL INFORMATION

Casting surfaces have a random, irregular pattern, whereas machined surfaces often have a cyclic character. This is why it is more important for castings to consider 3D areas instead of just relying on 2D line samples and to consider the spatial relation of the sample points. Spatial information means considering not only the height of a point (commonly z coordinate) but also its x and y position. Equations (1) and (2) represent the Roughness Average (*Sa*) and the Root Mean Square (*Sq*).[13] Both equations only consider the z-values of the points recorded, without considering the x and y-values. Therefore, any surface that has points with the same z-values produces the same *Sa* and *Sq* value no matter how these points are distributed on an x-y plane. Overall, calculating the *Sa* or *Sq* value only utilizes 33% of the information acquired during a surface scan.

$$Sa = \frac{1}{MN}\sum_{k=0}^{M-1}\sum_{l=0}^{N-1}\left[\mathrm{z}\left(\mathrm{x_k},\mathrm{y_l}\right)\right] \qquad \textbf{Eqn. 1}$$

$$Sq = \sqrt{\frac{1}{MN}\sum_{k=0}^{M-1}\sum_{l=0}^{N-1}[z(x_k, y_l)]^2} \qquad \textbf{Eqn. 2}$$

The method presented here considers the x and y coordinate as well as the z coordinate. The final result is derived from a variogram. Previous applications of variograms include the characterization of soil surface roughness.[14-16] Equation (3) shows that a variogram calculates one-half the mean of the squared height differences for points at a specified distance.

$$\gamma(l) := \frac{1}{N}\sum_{x}[z(x) - z(x+l)]^2 \qquad \textbf{Eqn. 3}$$

To create a variogram this calculation has to be done for all distances that one wants to visualize. The variogram itself often looks similar to the square root function. Variograms consider spatial information through distance calculations based on x and y-values to determine the height differences for a distance bucket. Because roughness values are usually measured in mm and not mm,[2] the square root of everything on right side of Equation (3) is calculated. Some changes were also made to accommodate the approximate (non-continuous) calculation and come to the Equation (4).

$$v(d) := \sqrt{\frac{1}{2N(d)}\sum_{N(d)}\left[z_i - z_j\right]^2} \qquad \textbf{Eqn. 4}$$

Where $N(d)$ is the number of pairs for the distance d which has a negative tolerance s (step size) and $v(d)$ is the value on the variogram for distance d. Distance d is the Euclidian distance on the XY-plane. Several methods were tested to determine a single quantitative value from a variogram. In one of the study's characterizing soil surfaces, the correlation length was used to classify surfaces and was determined by finding the point of intersection of two lines [14]. One line is tangent to the beginning of the variogram and the other tangent to the end of the variogram. The y-value of the point of intersection is then used to classify the surface. The implementation of this metric can be seen in Figure 3. The linear dashed lines are tangent to the variogram at the beginning and end. Their intersection (1.2, 0.08) marks where the correlation length is determined. This correlation length was tested for casting surfaces, but it was decided to be not as effective because of its sensitivity to outliers, specific variogram forms, and boundary effects. The method that seems to be most promising calculates the average of distance buckets in the range of the evaluation length, of which 0 – 5 mm seemed to be most promising (5).

$$S_{VR}(e) = \frac{\sum_{N(b)} v}{N(b)} \qquad \textbf{Eqn. 5}$$

Where $N(b)$ is the number of distance buckets b within the evaluation length e, v is the result of (4) for each bucket and S_{VR} is the variogram roughness. The result of this method is then able to represent the surface roughness of a specific surface. The vertical solid line in Figure 3 marks the evaluation length, while the horizontal solid line marks the variogram roughness.

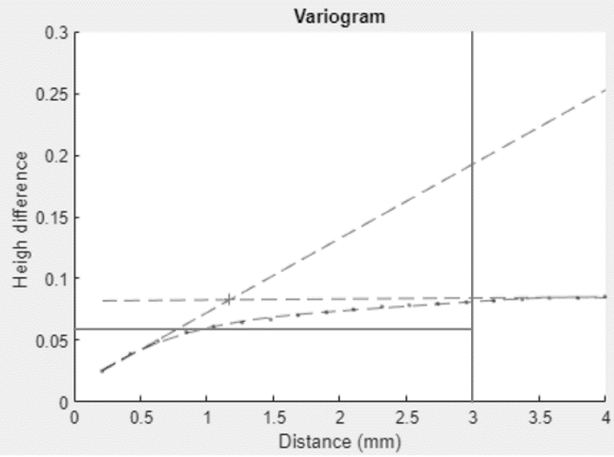

Figure 3. Variogram with correlation length and variogram roughness (0-3 mm).

UNDERLYING GEOMETRY

Surface characterization includes several parameters, including roughness and waviness. Roughness is made up of high-frequency components, whereas waviness is made up of medium frequency components. When calculating the surface roughness of a profile, the waviness is filtered from the recorded data and only the roughness profile is used to calculate the surface roughness parameters such as *Ra* or Rq.

The differentiation between roughness and waviness in two dimensions can be achieved by high and low pass filtering, but this is not easily translatable to three dimensions. What is known as waviness in two dimensions, is referred to as underlying geometry in three dimensions. The determination of underlying geometry for castings is more complicated than for machined surfaces because of the inherent dimensional variability. For example, surfaces designed as planes will have some curvature after the casting process because of mold wall movement and differences in shrinkage. Thus, whereas the CAD file may be used to establish the underlying geometry on a machined part, it cannot be used to estimate the underlying geometry of a casting surface. A method is needed to estimate the underlying geometry which then can be used to calculate a roughness value. The method chosen to determine the underlying geometry for this study is utilizing a grid of planes, which have sides equal to the sides of the surrounding planes. Figure 4 shows how this method works. In the first step of the method, a grid size is set; it was set to 5 mm in both x and y-directions. Next, the first set of z-values is calculated by determining the mean of the points in the area. Following this, quadratic polynomial functions are then fitted to the points in x and y directions. Subsequently, the functions are used to update the z-value of the grid. For every x,y coordinate the polynomial functions in x and y directions are multiplied by 0.25 and then added to the former z-value multiplied by 0.5. By giving the polynomial function and the old z-values 50% of the weight, the influence of abnormalities on the grid and the effect on the grid when the quadratic polynomial functions do not resemble the underlying surface can be reduced. The grid is then used to define small rectangular surface patches as in B in Figure 4.

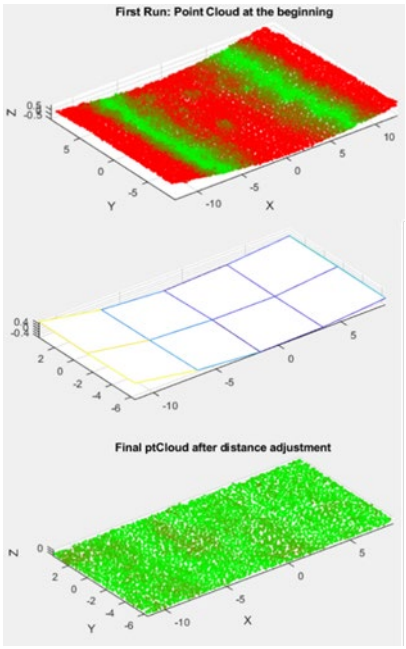

Figure 4. Example showing the underlying geometry and distance adjustment.

For every point, the closest surface patch is determined and then the distance from the point to surface is calculated. This calculated distance is then used as the z-value for the updated point cloud. Figure 4 shows the steps of the process starting with a curved point cloud, from this point cloud the underlying geometry is estimated and used to determine the z-values of the points. The color of the points in the point cloud in Figure 4 is determined by their difference to the mean z-value of the point cloud. Slight differences have a green color, higher differences a red color.

ANALYZING SCANS OF WHOLE CASTINGS

The described method does not work for more complex 3D scans such as scans of whole castings. The adjustments to the method are described as follows to potentially enable the analysis of complete castings and not just representative surface patches. Figure 5 shows an overview of the new method. In the beginning, an operator will perform a 3D scan of a part.

An operator then starts the program, and all following steps will be automatic. The resulting point cloud will be down-sampled, and its edges will be detected and removed from the point cloud. This is done because the underlying geometry detection does not work very well

around edges producing errors. After the edges are removed, clusters are extracted.

For each cluster, the underlying geometry (in the form of a mesh) is estimated, and then the point to mesh distances is determined.

Once the point to mesh distances for all clusters is calculated, the distances are used to determine the variogram roughness of the scanned surface. Then the abnormalities are detected based on threshold values and. the local roughness value. After the abnormalities are detected, they can be removed from the point cloud and then the underlying geometry detection can be repeated without being influenced by abnormalities. This can then be used to update the point to mesh distance and provide variogram roughness value not influenced by abnormalities As seen in Figure 5, the first step is to acquire a point cloud of a casting. To achieve this, the casting is scanned by a laser scanner or other 3D sensor.

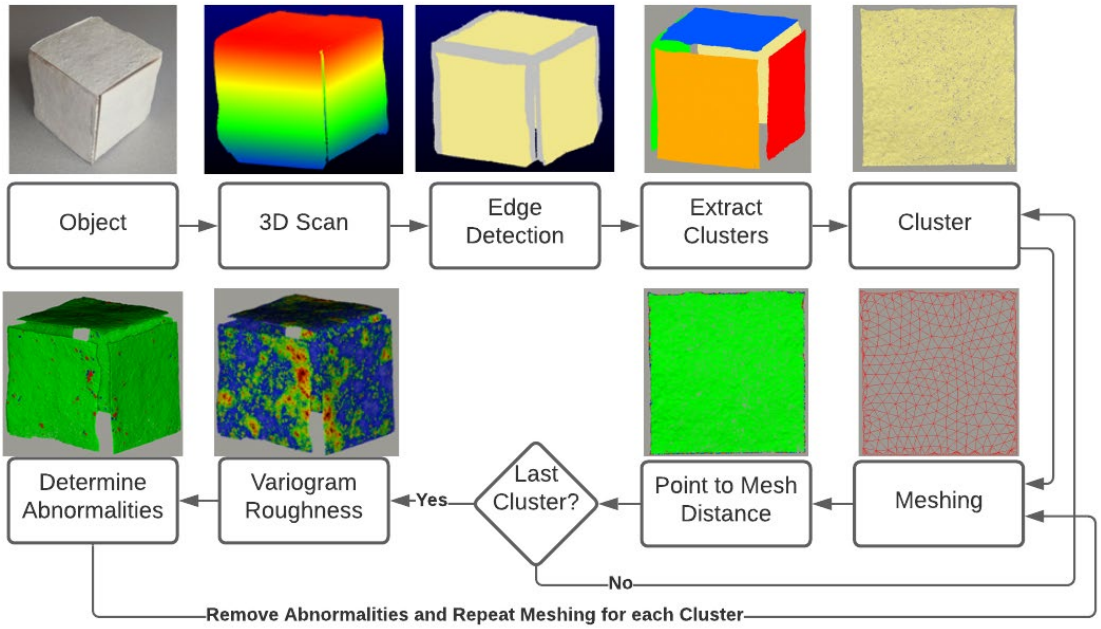

Figure 5. Flowchart showing the overview of the method that was developed.

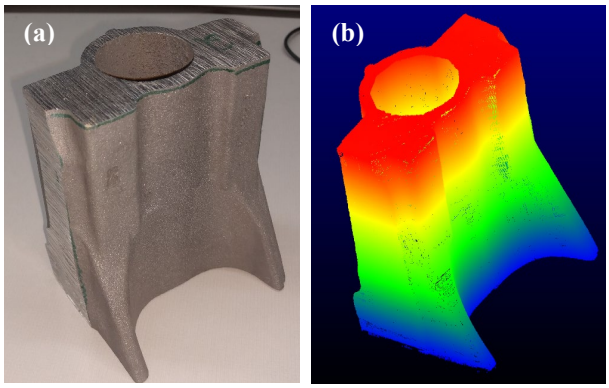

Figure 6. Image of a sample casting (a) and scanned point cloud colored from blue to red based on the z-value (b).

Sparse point clouds will reduce the accuracy of the surface roughness calculations, so a more dense cloud is captured, which is later down-sampled. Figure 6 shows an image of a casting and a 3D scan of that casting.

For the implementation of the surface roughness method, the Point Cloud Library (PCL) and the Computational Geometry Algorithms Library (CGAL) were used. As the names may suggest, the PCL contains many algorithms for the manipulation and analysis of points clouds,[17] and CGAL focuses more on geometry and surfaces.[18] The new method follows Algorithm 1, seen on the next page. The following will describe each step in the algorithm.
At the beginning, the dense input point cloud is down-sampled with a voxel grid filter. The voxel splits space into many voxels, which are small volumetric cubes. For each voxel, all points within the voxel have approximated by the centroid. For this application, the point cloud was down-sampled with a voxel edge length of 0.2 mm. After the point cloud is down-sampled, the edges of the

geometry are determined. This is done because, without removal of the edges, especially around the corners, the points are further away from the mesh, as seen in Figure 7. This shows that the underlying geometry detection is not very accurate around the corners. It smooths the sharp edges and thus results in higher distances between points and the mesh around the edges. For an accurate surface roughness calculation, accurate points to underlying geometry distances are necessary. Therefore, the points around the edges need to be avoided for the roughness calculation.

To be able to avoid these inaccuracies, one needs to identify what points are around the edges. The Canny edge detection algorithm[19] is a widely used method to identify edges in images. An implementation of the Canny edge detection for PCL exists[20] as long as the point cloud is organized and contains color information. An organized point cloud stores each point in a matrix similar to an image and is often the result of a 3D sensor like the Kinect. The point clouds used as an input for this application are mostly unorganized point clouds. Thus, instead of a canny edge detection algorithm, an algorithm for unorganized point clouds was used. This algorithm utilizes the eigenvalues of the covariance matrix based on the k-nearest neighbors to detect sharp edges.[21] Since the point cloud distribution is not necessarily consistent, the algorithm was slightly altered to use a radius search instead of a k-nearest neighbor search. The results of this edge detection can be seen in Figure 8. The gray points are points that are considered edge points, and all other points are yellow and can be used for the surface roughness calculation.

Algorithm 1 Surface Roughness Determination Algorithm

```
procedure SURFACE ROUGHNESS DETERMINATION
Downsample point cloud
Determine & delete edges
Extract Clusters
for all the Clusters do
        Optional: Grid filter point cloud
        Downsample mesh source point cloud
        Calculate normals of mesh point cloud
        Orient normals
        Orient normals away from point cloud center
        Delaunay-based surface reconstruction
        Dense isotropic remeshing
        Distance calculation between mesh and point cloud
        Remove points on mesh corners
        Calculate Variogram Roughness
end for
Combine Variogram roughness results of Clusters
Determine Abnormalities
end procedure
```

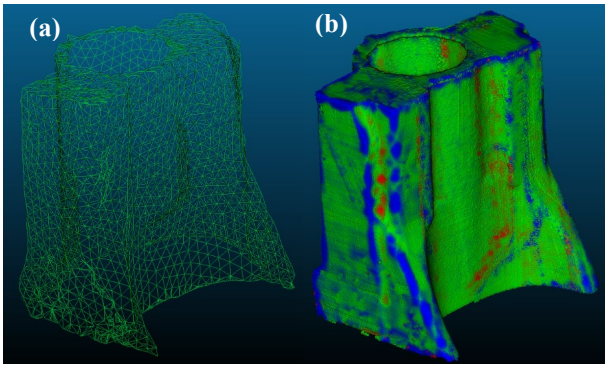

Figure 7. Surface mesh representing the underlying geometry (a) and colored point cloud based on the distance to the mesh (b). Green close to the mesh; blue and red far from the mesh; red outside of the mesh, blue on the inside.

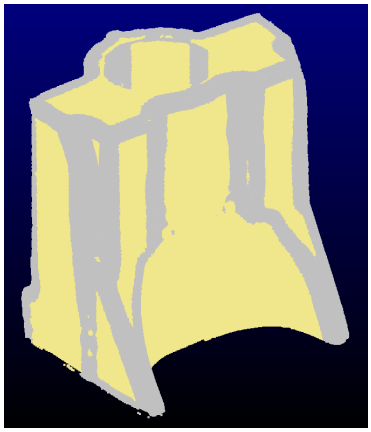

Figure 8. Sample casting with edge points colored gray, and all others colored yellow.

Once the edges are determined, they are removed from the point cloud. As can be seen in Figure 8 , the edges split the point cloud into multiple smaller areas. Thus, the point cloud is next separated into multiple clusters, which all fulfill a separation (d = 10 mm) and minimum size (n = 5000) criteria.

Next, for each cluster, a couple of calculations take place. Since the variogram roughness method is sensitive to noise, optional grid filtering can be performed. This grid filter can remove more noise from the point cloud data than the voxel grid filter with voxels of equal edge lengths. This grid filter aligns the cluster with the best fitting plane and then utilizes a voxel grid filter where the x and y edges are equal to the down sampling value while the z value is much higher. This way, all points within one x-y grid are combined to one point. This filter works well as long as the point cloud clusters size in the two main dimensions (x & y) is much larger than in the third dimension (z).

Next, a point cloud for the mesh is down-sampled even more for the upcoming meshing. The point cloud's normals are then calculated and oriented in the following step utilizing the orientation normals method from CGAL.[22] Utilizing a greedy Delaunay-based surface reconstruction algorithm,[23] a dense mesh is created of the point cloud with oriented normals. This densely meshed surface is remeshed to create a uniform mesh surface with a goal edge length of 5 mm. The remeshing is performed by utilizing the isotropic remeshing algorithm[24,25] implemented in CGAL. The reconstructed surface will be considered the underlying geometry of the casting and represented as a mesh. In the next step, for each point the closest point on the mesh and the distance to the closest point on the mesh is calculated. This is one of the computationally most expensive operations. The mesh may not cover all points in the point cloud, resulting in high distance results for these points. Thus, these points are removed from the point cloud.

To be able to determine the variogram surface roughness value, both the distance from point to underlying geometry and distance from point to point are important. The distance from point to underlying geometry was previously determined. The points for the point to point distance will be the corresponding closest points on the mesh determined in the previous step. The distance from point to point is necessary to consider spatial relationships. The variogram, which is used for this method, plots the height difference between points for different distances. If the points are closer together, the height difference is usually lower. There are two common ways the distance between the points can be determined. The easier of the two methods is just determining the cartesian distance between the two points. To calculate the cartesian distance, only the location of both points is necessary. The second method is using the shortest distance along the mesh to connect the two points. This is more accurate for our purpose because, for the relationship between the points, the surface distance has more meaning than the cartesian distance.

Both methods were implemented for the variogram roughness calculation. The surface distance measurement is the more accurate one, but on a computer with a six core processor (i7-8850H), the calculations took over an hour for the example part and are thus far too long to be feasible. The calculation of the surface distance is much more computationally expensive than the cartesian distance because a search algorithm has to determine the closest path between the two points on the surface. The point clouds for the surface roughness calculation can quickly have millions of points. For each one of those points, the distance to thousands of points has to be calculated. Thus, the computational time for this distance calculation is high.

In practice, the cartesian distance will be used to evaluate the distance between two points on the surface. The biggest inaccuracies for the cartesian distance calculation occur around edges. By not using edge points for the roughness calculation, the cartesian distance is a good compromise between calculation time and accuracy.

Once the distances between points on the surface as well as the point to surface distances are determined, the variogram roughness value can be calculated for each point. These variogram roughness values can color the point cloud and present the local roughness on the point cloud. One can see examples of this in the result section. This can help identify areas on the surface of different roughness. After the variogram roughness values for all clusters are calculated, they are combined to determine the scanned surface's final roughness value without its edges.

The described method would provide one overall roughness value, but a casting might have a variety of different surface roughness spread over the surface. Further, the underlying geometry detection is not perfect; thus, more accurate values will likely be achieved if analyzing a simple surface like a plane. For both cases, it may be advantageous to cut out a smaller section and determine the smaller section's surface roughness.

After the local roughness values were determined, the information can be used to determine abnormalities on its surfaces. This can be done by comparing the local surface roughness values with the overall roughness value. If, for example, a local surface roughness is twice as large as the final roughness value, it could be considered abnormal. The method differentiates between abnormalities where material is in excess or missing by utilizing the relationship between the oriented normal vectors and the center of the point cloud.

PORTABLE MEASUREMENT DEVICE

Previous variogram roughness implementations did not integrate with hardware directly. This made it necessary to export and clean up a point cloud before evaluating the surface roughness. To evaluate the possibility of utilizing a portable device to quickly and reliably assess the surface roughness of a representative section of a casting, a prototype was built. The device was constructed around a 3D scanner which needs to fulfill certain criteria. These criteria include the scanning area (> 50 x 50 mm) and accuracy (<0.035 mm) as well as being able to capture data quickly without the operator having to move the sensor. Not having to move the sensor manually should reduce the variation when scanning the same surface multiple times. The sensor chosen in this paper is a Micro-Epsilon surfaceCONTROL 3D3510-80 with x-y-resolution of 35 - 45 µm, a z-resolution of 1.0 µm and repeatability of < 0.4 µm.[10] The scanning area ranges from 55 mm x 42 mm at 110 mm and 75 mm x 54 mm at

the far range (150 mm). A housing for the sensor was. designed to mount the sensor as well as a touchscreen for control and information output. The housing has four legs, which keep the sensor within the scanning range, Figure 9. The inside corners of the legs are only slightly larger than the scanning area so that they can be used for aiming the device and thus analyzing the desired surface, Figure 10.

Figure 9. Prototype for areal roughness measurement of castings.

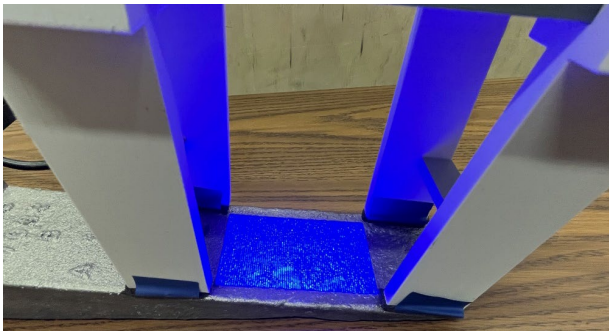

Figure 10. The rectangular scanning area is highlighted in blue.

RESULTS/DISCUSSION

ANALYZING SURFACE SECTIONS

This first study focuses on analyzing the results of the variogram without abnormality removal or underlying geometry detection and comparing them with other popular roughness values. This also shows the difference between a roughness value that considers spatial information and one that does not.

For this study, four test point clouds were created that have very similar Root Square Mean Height values. All point clouds have the same amount of points that were spread over the same x/y grid. The four created surfaces, shown in Figure 11 were:

- A cloud with randomly distributed z-values.
- A cloud with a zigzag pattern (z-values increase and decrease linear in y-direction but stay constant in the x-direction).
- A cloud with points on two planes on different levels (levels have different z-values).
- A cloud with points on a plane that has a slope (z-values increase linearly in y-direction but stay constant in the x-direction).

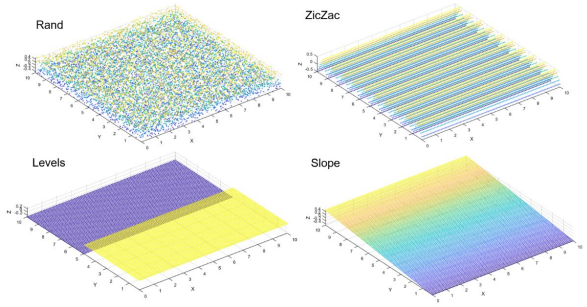

Figure 11. Figures showing the created test point clouds.

These point clouds were used as input for the surface roughness calculation and the values *Sa*, *Sq* and multiple Variogram roughness values with different evaluation lengths were determined, Figure 12. Underlying surface detection and abnormality detection were not active.
The results of the test point cloud in the form of photographs of the variograms are presented in Figure 13. When looking at the variogram from the random point cloud one can see that the mean difference between two points for all distances is about the same. This is expected since points for all distances are random. If one looks at the variogram of the zigzag point cloud one is able to see this zigzag in the variogram as well. For higher distances, this zigzag correlation becomes less visible and that is because for longer distances there are more points that influence the variogram roughness. The third variogram shows the result for the bi-level example and the fourth the sloped point cloud example. For both point clouds, it is valid that the higher the distance between two points the higher is the distance variation between them. For the bi-level point cloud, there is a drop off in the slope of the variogram at about 5 mm and that is because the point cloud has an x and y size of 10 mm. Figure 13 also shows the influence of the evaluation lengths for the variogram roughness. The evaluation length is the range of variogram points that are averaged to determine the variogram roughness. A lower evaluation length causes a smaller roughness value. The sensitivity seems to increase with a higher variogram roughness value.

The results in Figure 12 show that the *Sa* and *Sq* values are not able to differentiate between these test clouds very well. Whereas the variogram roughness values are able to differentiate between these surfaces. One can notice that

the *Sq* value and the variogram roughness value are the same for the 'random' point cloud. This is the case because these values are based on the root mean square and in the random cloud, no information is stored in the x,y coordinates. The *Sa* value is different because the square root of the squared z-values is not taken. The difference between the non-spatial values and spatial values becomes bigger when one goes form the 'zigzag' point cloud, to 'levels' and finally to the 'slope' point cloud. Another item to notice is that the difference between non-spatial values and spatial values is the greater the smaller the evaluation length of the variogram roughness.

To further investigate if the method produces results that agree with the current measuring method, a ranking comparison test was performed. Since this is a new method to classify surface roughness and there is not an established digital method, one cannot just compare the values of the new method with the values of an established method. The current method is classification through visual inspection by operators. Human operators are not perfect at determining the surface roughness of a casting, but if the method should be used in the industry it has to agree in some ways with the human results on surface roughness.

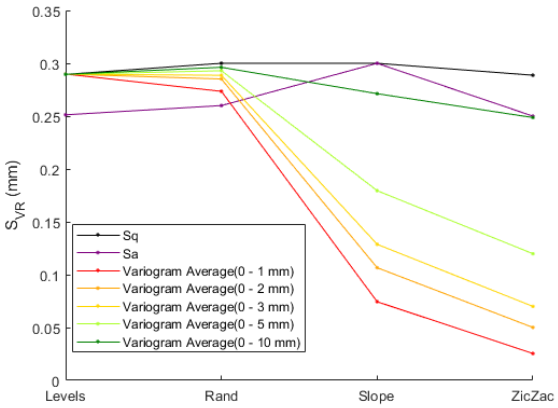

Figure 12. Figures showing the variogram for test point clouds.

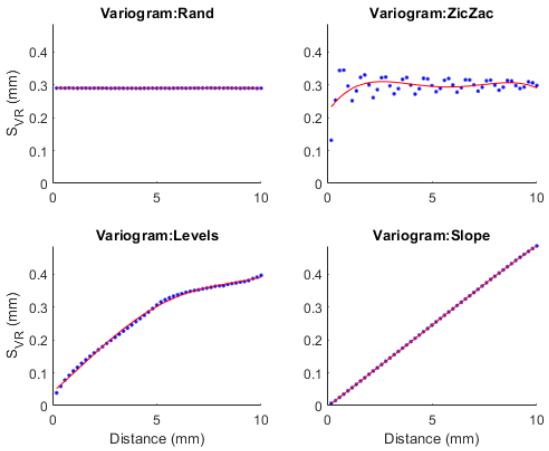

Figure 13. Results for test point clouds.

It was assumed that human operators should be good at a pairwise comparison between plates and thus, should be able to order plates from lowest to highest surface roughness. Nineteen replicas of real casting surfaces were used, and four subjects ranked them. Some of these plates had abnormalities on them which were marked, and the operators were told to not consider them in their surface roughness rankings. The replicas were laser scanned, the abnormalities that the subjects were told to ignore were digitally removed, the surface variogram roughness values were calculated, and were ranked by the variogram roughness values.

Figure 14 and Figure 15 present the results. Figure 15 shows that for some replicas (e.g., replica 11) the consensus between operator and program is good. For other replicas, such as replica 16, one operator gives it the ranking 3 and another ranking 12. From Figure 14 one can conclude that there is some overall consensus. A correlation between the mean operator ranking and the digital method (program) with the Spearman's Rank Order Correlation was checked and the test concluded that there is a highly significant correlation (r_s=0.76, $P <$ 0.001). The agreement between the variogram roughness values and the operator means supports that the method is working similar to an operator. This experiment also showed the disagreement of the operators. Often when there was disagreement between the operator and the methodology there were abnormalities that the operators were supposed to exclude but likely subconsciously considered in their evaluation.

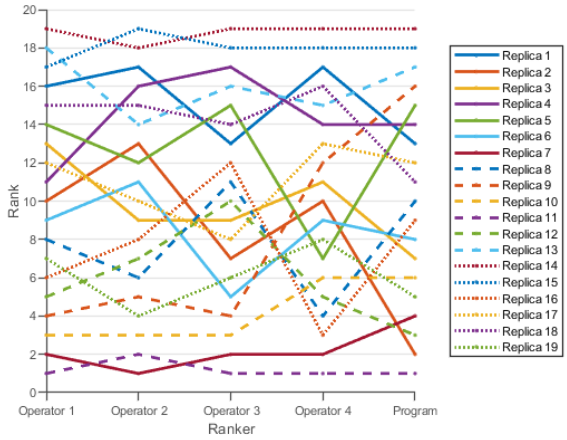

Figure 14. Rank comparison: ranker vs rank.

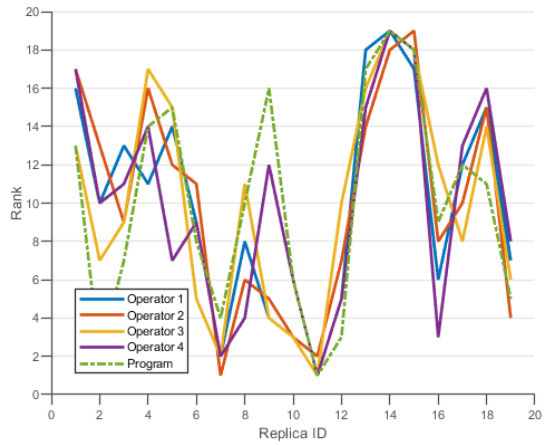

Figure 15. Ranking comparison of the test plates by operator: plate number vs rank.

To be able to determine if the variogram roughness value is able to classify casting surfaces satisfactorily, the Surface Variogram method, designated as *Svr,* was used to calculate the roughness values of SCRATA and GAR-C9 plates, which are the current standards in surface roughness determination of castings. To create the boxplots in Figure 16, eight scans of every surface were taken and the variogram roughness for an evaluation length of 0 – 5 mm was calculated. The abnormality detection was not active.

One is able to see that the rougher surfaces cause a higher variogram roughness value. For these analyzed surfaces there was also no overlap of the boxplot antennas for the different surface roughness. This means that a threshold value can be determined to differentiate the levels of surface roughness. For instance, a threshold value for the SCRATA A2 plate could be placed at 0.048 mm and 0.063 mm. Based on these threshold values, surfaces can be matched with a SCRATA roughness level.
For example, if a surface has a roughness value of 0.04 mm it would be considered A1, for 0.055 mm A2. It also shows that the method with the specific scanner is repeatable enough to differentiate between the roughness levels. Because of the accuracy of the scanner (3D measuring arm: ±34 µm, laser line probe: ±35 µm)[26]), the smoothest GAR-C9 surface that was analyzed was the 200 microinch RMS. Smoother surfaces were too smooth to be able to differentiate in between based on the laser scan data. If data from a 3D scanner with higher accuracy is available, the method should be able to differentiate between the lower GAR-C9 roughness levels.

ANALYZING SCANS OF WHOLE CASTINGS

The following results are regarding the *Svr* model development which is able to analyze whole castings. The SCRATA comparator plates were used to validate the implementation of the method to analyze three-dimensional castings rather than just flat surfaces. Rubber molds (3 x 3 in) of the SCRATA plate sections were used to create plastic copies of the SCRATA plate sections, Figure 17. These squares are used to create epoxy copies of the SCRATA plate molds.

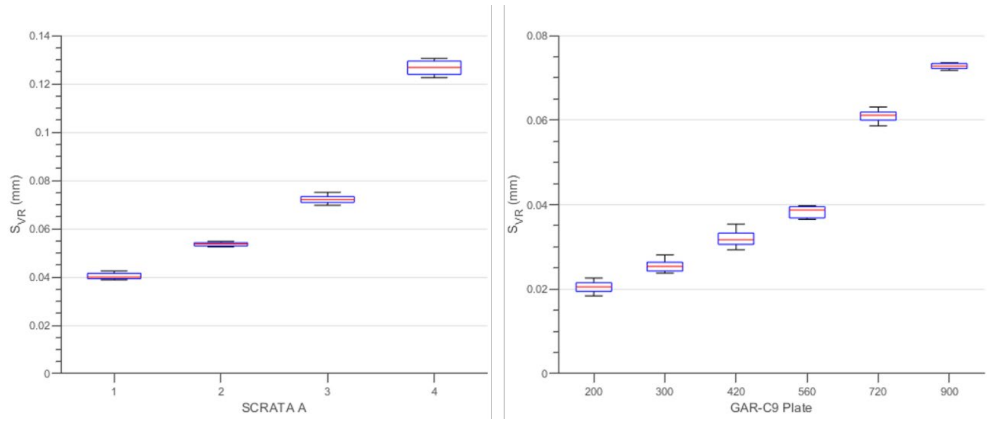

Figure 16. Variogram results for SCRATA A1-A4, GAR-C9.

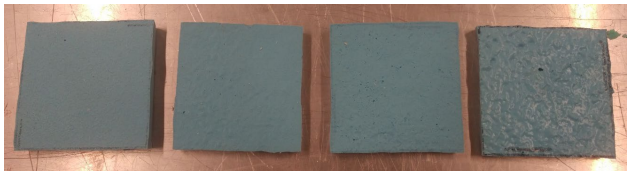

Figure 17. Rubber molds of SCRATA A1-A4 comparators.

Five of the plastic copies are assembled to create a three-dimensional cube where all sides are one of the four SCRATA surface roughness levels (A1, A2, A3, and A4), see Figure 18 and Figure 19. The cubes will have discontinuities/gaps around the corners, but the edge points are not used for the roughness calculation and therefore, should not impact the results. Since only a square section of the SCRATA plates is used, and inaccuracies in the copies exist, the roughness results are not expected to be exactly the same as for a SCRATA plate but similar.

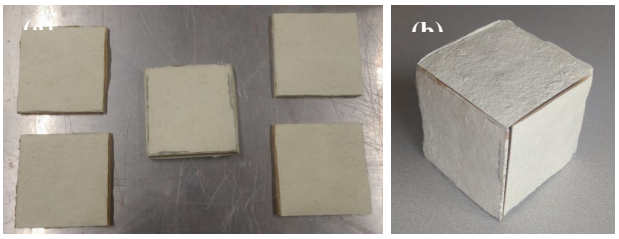

Figure 18. 5 SCRATA A3 copies (a) and SCRATA A3 cube (b).

Figure 19. SCRATA cubes A1- through A4.

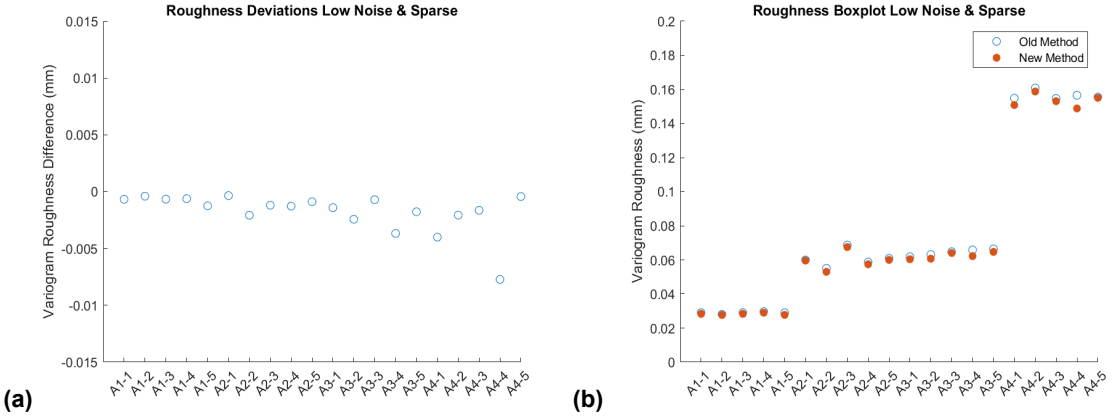

Figure 20. Roughness results for the sides of SCRATA cubes analyzed separately (Low Noise & Sparse).

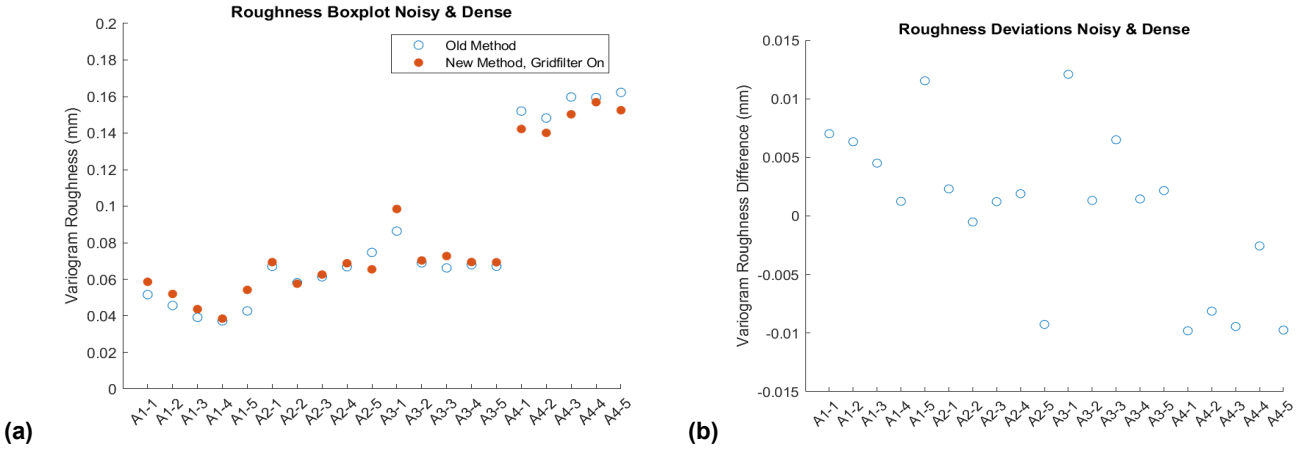

Figure 21. Roughness results for the sides of SCRATA cubes analyzed separately (Noisy & Dense).

To determine if the previous validated method and the new method are able to produce similar results, the SCRATA cubes were scanned. These scans were gathered with two different 3D scanners, one of which had very dense but noisier results. In contrast, the other scanner's results were defined by low noise but a sparse point cloud with a non-uniform point distribution similar to a meshed surface. For the first part of the test, each scan of a SCRATA cube was cut into five smaller scans. Each smaller scan is one side of the cube. These 20 scans were then analyzed using the previous MATLAB method for patches and the new method implemented in C++. For all following tests for both methods, the point clouds were down-sampled to 0.2 mm, and an evaluation length of 5mm was used for the variogram roughness calculation. Further, for the underlying geometry detection, a surface patch size of 5 mm was chosen. For the old method, this means a grid size of 5 x 5 mm, and for the new method, a goal edge length of 5 mm for the triangles. In addition, both methods did not utilize abnormality detection and removal. This test is supposed to investigate the variation between the results if both methods receive the same input. The results can be seen in Figure 20 **(a)**, where A1-1 through A1-5 are scans of the five sides of the SCRATA cube A1. For each scan, two results are displayed. The filled circle represents the new method, while the unfilled circle represents the previous method. One can see that the results are very similar.

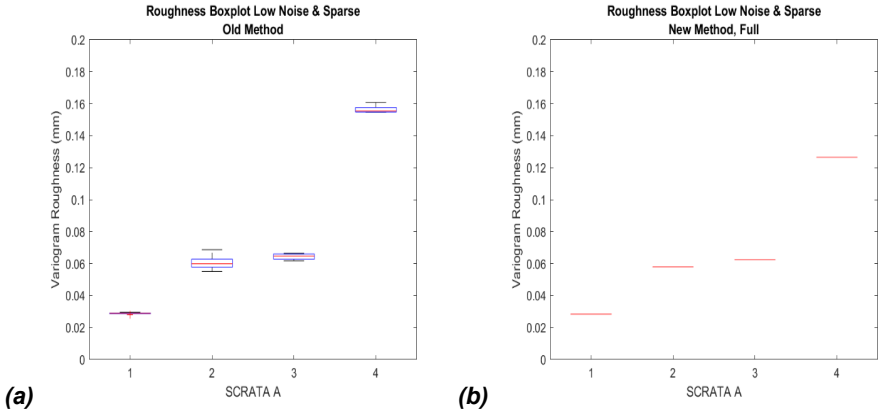

(a) (b)

Figure 22. Low Noise & Sparse: Roughness result comparison between the old (a) (five results for each roughness level) and new (b) method (one results for each roughness level).

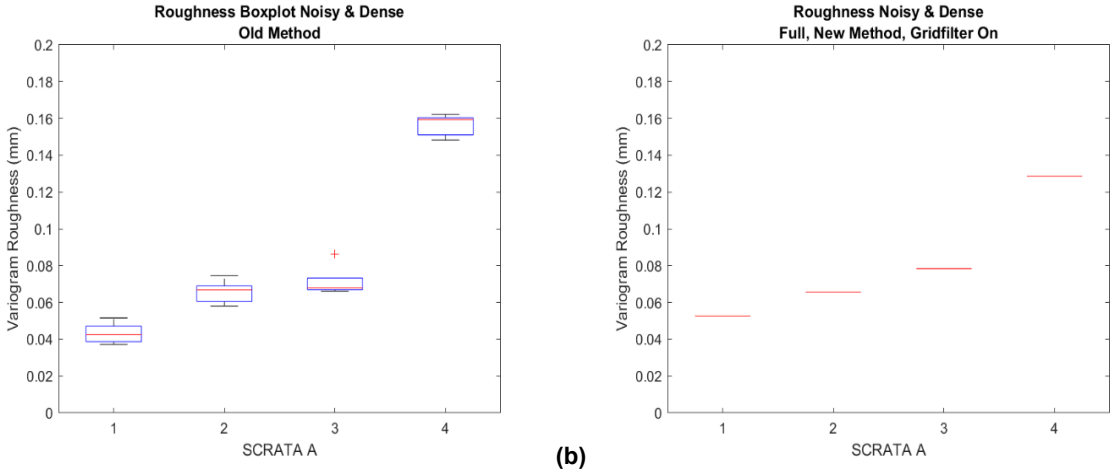

(a) (b)

Figure 23. Noisy & Dense: Roughness result comparison between the old (a) (five results for each roughness level) and new (b) method (one results for each roughness level).

Most of the time, the previous method produces slightly rougher results. **(b)** presents the deviation between the previous and new method. A positive deviation corresponds to the result of the previous method being larger. **(b)** further shows that the deviations are all smaller than 0.008 mm, all except one even smaller than 0.005 mm.

Figure 21 presents the same data as Figure 20 but for the scans with the dense but rather noisy data. One can see that the differences between the old and new method are larger in this case.

Since the point cloud is noisy the new method utilizes the grid filter. One can see that the variations are larger than for the point cloud with low noise. The maximum deviation is now closer to 0.013 mm. While Figure 20 shows the results of the SCRATA cube sides analyzed individually for both methods, Figure 22 **(b)** shows results where a scan of the whole cube was used as an input for the new method. The boxplots in Figure 22 **(a)** present the results of the four different SCRATA cubes where the five sides are analyzed separately by the old method.

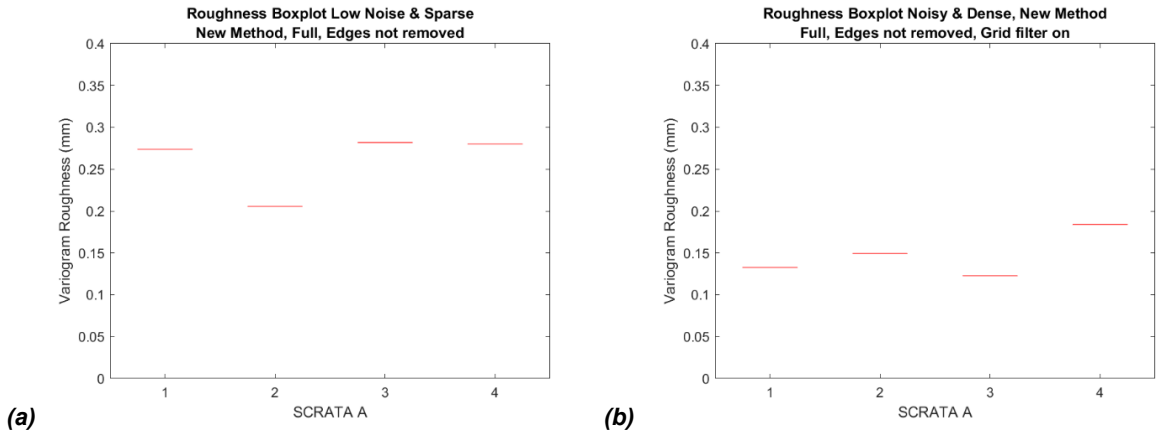

(a) *(b)*

Figure 24. Roughness result without edge removal Low Noise & Sparse (a) and Noisy & Dense (b).

The new method uses the whole scan and then removes the edges automatically, while for the old method, the edges are removed manually so that they can be analyzed separately. Since the input will differ, some variation is to be expected. Comparing **(a)** and **(b)**, one can see that the results are similar, but especially the results for the SCRATA A4 cube are different. This can be explained by issues in the edge detection. The edge detection uses the curvature in an area to find edges. While this works very well for A1-A3 surfaces, A4 surfaces themselves have high curvature, which causes the new method to classify part of the A4 surface as edges and not use them for the roughness calculation. Since the areas with high curvature are also areas where more considerable height differences between points are to be expected, this overall reduces the roughness reported by the new method for the SCRATA A4 cubes.

Again Figure 23 shows the same data as Figure 22, but for the scans with the dense and noisy data. Comparing the results, the variation between the five sides of the cubes is a little higher for the noisy data, and the results for the lowest roughness level A1 are higher in general.

In the results presented above, the cubes' edges were removed either manually or with automatic edge detection. Figure 24, on the other hand, shows the roughness results achieved by the new method without removing the edges, to check if error is introduced if the edges are not removed. **(a)** presents the results for the scans with low noise but sparse data while **(b)** shows the results of noisy but dense data. The results are not close to the previous method results, as seen in Figure 22, which shows that the edge removal is necessary because of the meshing operation's inaccuracies.

Similar to how scans are compared to CAD files for dimensional analysis, the point clouds can be colored based on the local variogram value to visualize roughness variation of the surface. This can be useful to identify areas in which subsequent finishing operations like grinding are necessary. Figure 25 presents the variogram colored point clouds for the SCRATA A1 through A4 cubes. The coloring scheme can be seen in Table 1 and is based on previous results acquired with the old method.

Table 1. Variogram Color Scheme (Between Values, Colors are Interpolated)

Local Variogram Roughness Value	Color	SCRATA Equivalent
0 mm	White	-
0.04 mm	Blue	A1
0.055 mm	Green	A2
0.072 mm	Yellow	A3
0.13 mm	Red	A4
0.2 mm	Black	-

From Figure 25, one can see the differences between the roughness levels. While A1 and A4 are very different, the color differences between A2 and A3 are much smaller. This matches the roughness results shown in the previous Figures.

Figure 26 shows an example of a cube where the sides do not have the same surface roughness. One can see a clear difference between the three facing sides. Utilizing Figure 25 or Table 1, one can determine that the left side's surface roughness is close to A1, while the top's surface roughness is close to A3 and the right side's surface roughness is close to A4.

The method also includes an abnormality detection that, similarly to the point cloud's variogram coloring, can assist in identifying abnormalities on the casting. In this case, abnormalities are defined as having two times the variogram roughness than the average variogram roughness of the casting. Excess material is marked in red, while missing material is marked in blue, Figure 27 shows an example of abnormality detection on the SCRATA cubes. Since they do not have any big abnormal areas, only small spots are marked.

PORTABLE MEASUREMENT DEVICE

To evaluate the possibility of utilizing a portable measurement device at foundries for roughness analysis, multiple gage repeatability and reproducibility (Gage R&R) studies on a variety of metal castings were performed. On multiple castings, rectangular surfaces to analyze were determined and identified by marking their four corners. During the Gage R&R study, the operators positioned the sensor over the area of interest and triggered the scan and roughness calculation by pushing a touchscreen button. The results were automatically saved for later analysis. The operators were instructed to align the inside corners of the legs with the marking on the casting and then keep the sensor as still as possible during the scanning operation because even though the scan takes less than a second, it is not instantaneous and movement during the scan can cause inaccuracies. From the time the roughness determination was triggered until the roughness was output it took around 15 seconds. During the first five seconds, the program established the connection with the sensor, took initial color images, adjusted the exposure times based on the initial color images, performed the 3D scan, and transmitted the point cloud. The roughness calculation was automatically performed once the point cloud was received from the sensor. The sensor had to be kept still during the first five seconds since the 3D scan did not start right after pressing start but around four seconds later. The movement of the utilizing the scanners' internal filters and a statistical filter removing point whose average distance to 10 other points was outside of four standard deviations from the mean sensor during that time would cause extraneous points in space and would dramatically increase the calculated surface roughness. To reduce the susceptibility of the 3D scanner to small movements during the scan, internal scanner functions were used to remove points with low confidence in their accuracy. Other ways to remove such points could be statistical filters, but statistical filters can also remove a lot of good points. In the end, a good compromise was found for the small movements during the scan which included flexing of the sensor housing from changing contact pressure (housing was 3D printed from PLA), as well as from shaky operator hands often in combination with situations where only three of the four legs of the sensor contacted the casting.

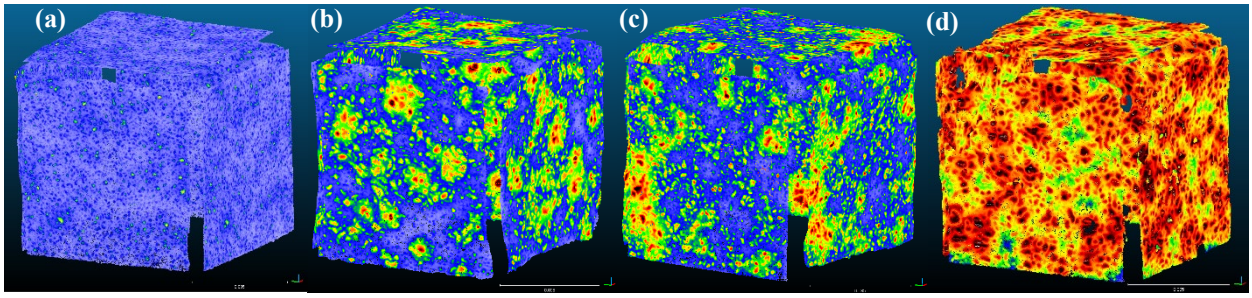

Figure 25. Variogram colored SCRATA A1 (a) through A4 (d) cubes (Low Noise & Sparse).

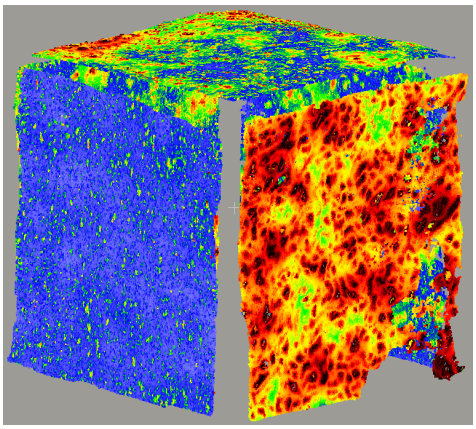

Figure 26. Variogram colored cube with different sides. Left-facing side A1; right-facing side A4; top A3.

Finding a relatively stable position for the sensor, whereas as many of the four legs as possible were in contact with the casting, combined which a constant pressure applied to reduce the effect of shaky hands, helped lessen the movement during the scan. Nonetheless, as will be shown throughout the four gage R&R trials, some of the 3D scans were affected by movements. This is evident in the recorded point cloud as well as higher determined roughness values.

The first gage R&R study included seven castings with similar shapes but different levels of roughness. One flat rectangular area, roughly the size of the scanning area of the sensor, on each casting was chosen for roughness analysis. The areas were identified by marking the four corners. According to visual comparison, the roughness ranged from A1 to A4. For the gage R&R study, each of the three operators scanned the seven surfaces three times. Figure 28 shows the seven surfaces which were inspected.

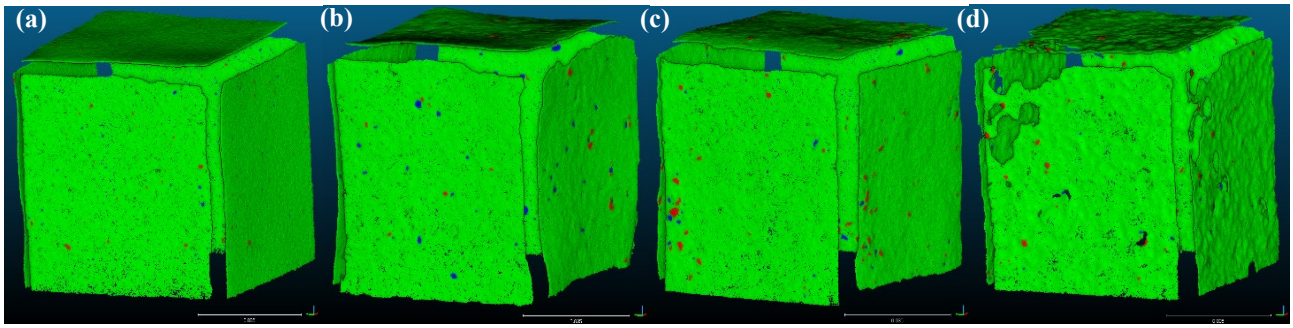

Figure 27. Detected abnormalities on SCRATA A1 (a) through A4 (d) cubes (Low Noise & Sparse.

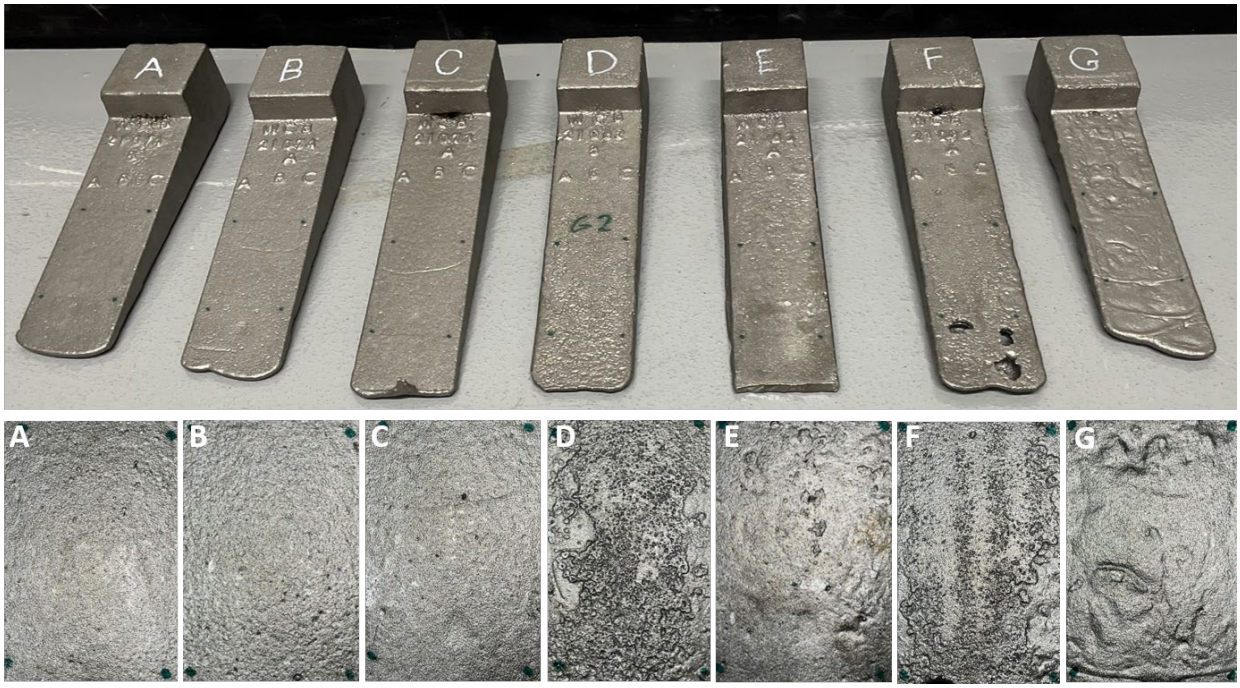

Figure 28. Gage R&R Study 1: Photographs of castings and the corresponding casting surfaces.

The results for the three operators can be seen in Figure 29. The low spread of the roughness values points to good repeatability. In total, for the three operators and the set of castings, repeatability of 0.0036 mm and reproducibility of 0.0017 mm were determined. Overall, the gage R&R was only 2.7%, but since this is determined based on the total range of roughness values for the given set of castings, which ranges from A1 to A4 it is less meaningful.

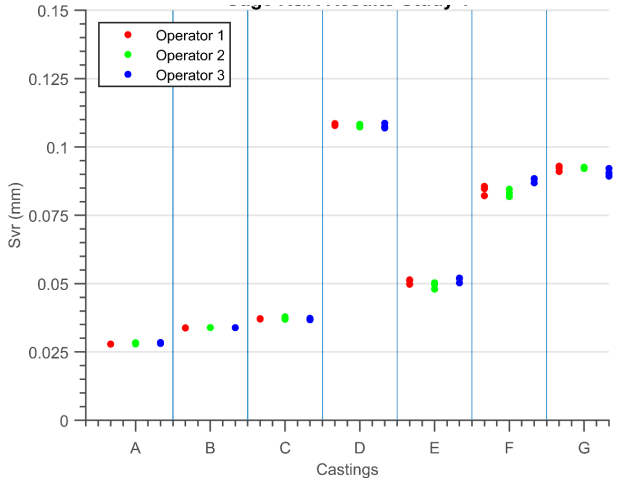

Figure 29. Results of the Gage R&R Study 1.

The second gage R&R study included eight castings with a larger variety of casting geometries. Figure 30 shows the overall shape of the casting, while Figure 31 shows a close-up of the inspected surfaces. For some of these geometries, the device had to be supported during the scanning operation (G1, G5, G7), while for others the device could stand without being held.

Figure 32 plots the results of the second gage R&R study. The results again show very repeatable results for most surfaces. Surfaces G5 and G6 had the most variation. Part of the variation can be explained by the more challenging positions the sensor had to be held in. For G5 the device had to be held nearly horizontal while G6 was an extremely rough surface, and only three legs were able to contact the surface at the time.

Figure 30. Photographs of the castings for the Gage R&R Study 2.

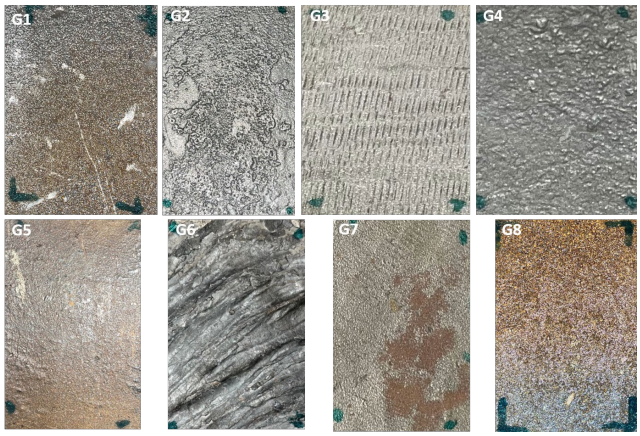

Figure 31. Gage R&R Study 2: Photographs of inspected surfaces.

In total, for the three operators and the set of castings, a repeatability of 0.0027 mm and reproducibility of 0.0021 mm were determined. Overall, the gage R&R was only 0.9 %. Based on visual inspection, the casting roughness ranged from smoother than A1 to rougher than A4.
The third round of gage R&R studies looked at multiple surfaces on the same casting, Figure 33. The surfaces were mostly randomly chosen, but visible surface anomalies were avoided to compare areas with similar surface roughness. The third round of gage R&R tests was split up between two castings, Study 3 focused on the casting called NR while Study 4 focused on the casting called NRN

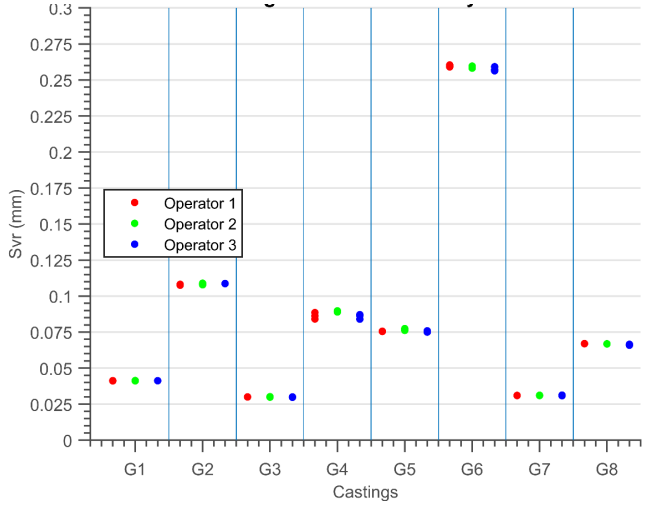

Figure 32. Gage R&R Study 2: Results.

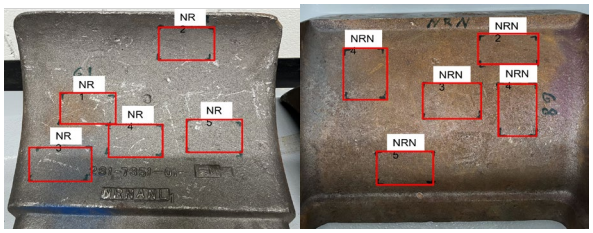

Figure 33. Test castings used in Study 3 with areas tested indicated.

While the surfaces of the casting NR all had about the same surface roughness (0.035 - 0.06 mm), the casting NRNs surfaces varied more (0.035 – 0.075 mm). Five areas on each casting were selected. Again, areas with visible abnormalities were avoided. Three operators scanned the ten areas three times each. Figure 34 and Figure 35 present the results for the castings NR and NRN, respectively. Study 3 repeatability of 0.0024 mm, reproducibility of 0.0011 mm, and gage R&R again was 8.5 % for study 3. A repeatability of 0.0027 mm, reproducibility of 0.0013 mm, and gage R&R of 6.12 % were determined for Study 4.

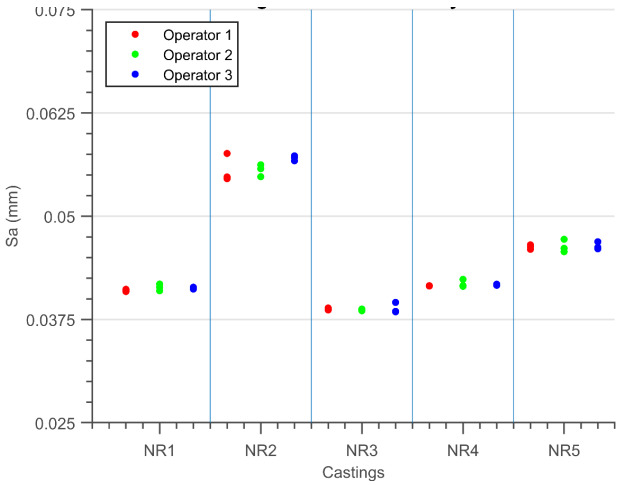

Figure 34. Gage R&R Results Study 3.

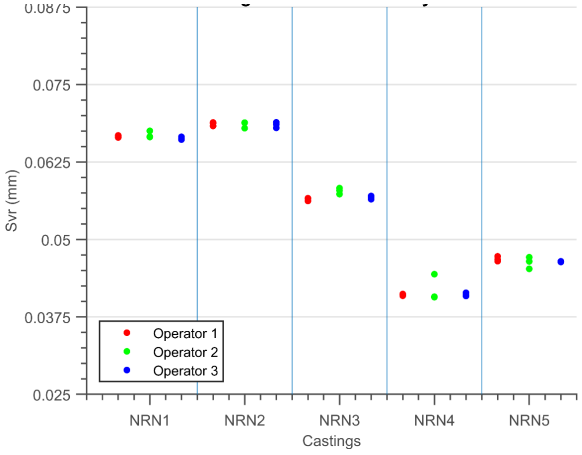

Figure 35. Gage R&R Results Study 4.

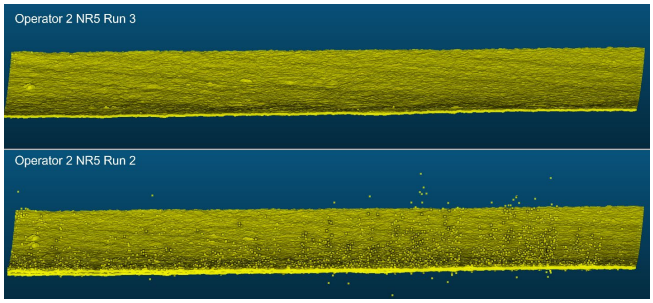

Figure 36. Comparisons of scans without excessive noise (top) and with excessive noise resulting from movement during scanning (bottom).

Figure 36 shows an example of the noise captured due to movement of the scanner. Operator 2 was asked to repeat the scans after being reinstructed on how to avoid movement during the scan. This led to a repeatability of 0.0024 mm, reproducibility of 0.0013 mm, and gage R&R was 8.7% for Study 3, Figure 37 and Figure 38.

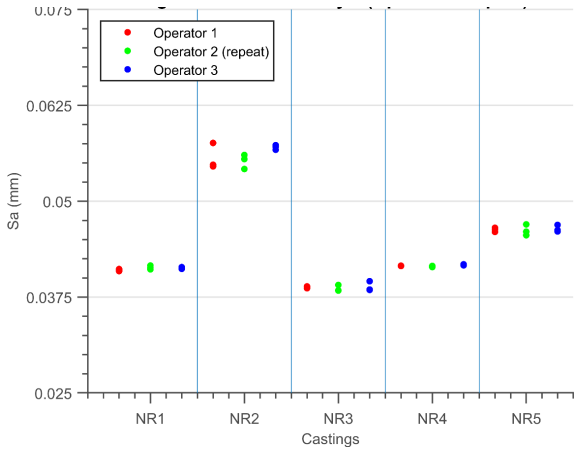

Figure 37. Gage R&R Results Study 3 (Operator 2 repeat).

A repeatability of 0.0017 mm, reproducibility of 0.0004 mm, and gage R&R of 3.6 % was determined for Study 4 using the data from operator 2 repeating the scans.

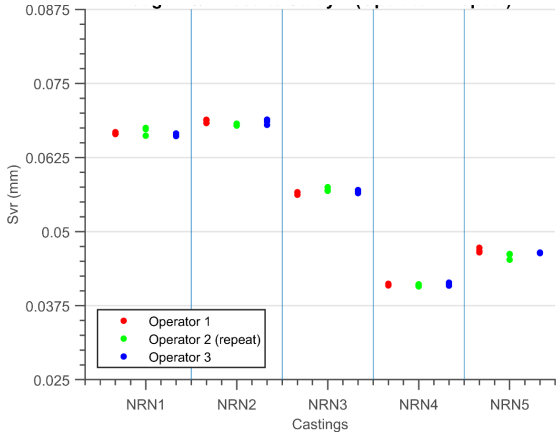

Figure 38. Gage R&R Results Study 4 (Operator 2 repeat).

SUMMARY OF WORK / CONCLUSIONS

ANALYZING SURFACE SECTIONS

Overall, the *Svr* method showed promising results in the objective surface classification. Lab tests showed its advantages to current digital surface roughness standards which it was able to outperform in differentiating between surfaces. Its ability to differentiate between current comparator plate standards means that it can potentially be used to classify surfaces similar to today's standards. It also showed improvements in the area of repeatability & reproducibility in comparison to the current standard visual inspection, which will be able to improve communication and reduce the disagreement between producer and designer. Furthermore, it showed that the correlation between the mean result of four inspectors and the objective method is highly significant. This indicates agreement with today's standard, which currently relies

on a human inspector. During this research, a MATLAB application was developed which is able to calculate the surface roughness automatically.

The results also showed the importance of the underlying geometry detection. A bad fit of the determined underlying geometry can cause higher roughness values as well as decrease the accuracy of the abnormality detection.

ANALYZING SCANS OF WHOLE CASTINGS

The tests showed that the method is able to produce comparable results for SCRATA A1-A3 cubes. The roughness results for the SCRATA A4 cube were comparable if the edges were removed manually. However, the automatic edge removal currently removed too much of the surface for A4 surfaces, which leads to lower roughness results than the previous method. Overall, this should be acceptable because castings with surfaces as rough as the SCRATA A4 plate are not very common. Nonetheless, one way around this would be to compare the scanned surface data with the castings CAD model. While this presents other issues as the casting does not match the CAD model perfectly, the variogram roughness method may be able to filter out the deviations between the CAD and actual casting geometry and still produce good roughness results.

This method's limitations further include that the method does not evaluate the whole casting since the edge surfaces are not evaluated. For most castings, this should nonetheless enable a roughness evaluation of most surface areas.

The roughness results from the two different inputs, one noisy and dense, the other sparse but less noisy, showed the importance of good scan data. Overall, the scan data with less noise was able to produce more consistent results. The method's ideal input data would be a dense point cloud, with uniform point distribution and low noise. The low noise scan data available to us did not have a uniform point distribution because of the smoothing taking place in the scanner's software.

Tests have also been performed with underlying geometry detection based on Bezier curves, but the results were, in general, worse than the underlying geometry detection presented above. Nonetheless, it would be advantageous to test more methods for the underlying geometry estimation and their influence on roughness results. With some further refinements, this surface roughness measurement method can be used to make the technique more accessible for casting producers and users since now scans of whole castings can be analyzed. It should be possible for the foundries to include the method to the geometric analysis of castings already taking place utilizing the same 3D scan. The method could also be used to identify areas on surfaces where a subsequent automatic finishing operation reduces the surface roughness or removes abnormalities.

PORTABLE MEASUREMENT DEVICE

This study was able to present a prototype of a portable device that can be used to determine the surface roughness of small surface patches. It was able to do so within a reasonable amount of time and with good repeatability and reproducibility. The gage R&R studies showed that the device was able to gather surface roughness information from a wide variety of surfaces. There are limitations to the surfaces that can be analyzed because of the ranges at which the sensor can perform surface measurements, but in practice, if simple geometries are being analyzed this is not an issue.

As could be seen, especially with the gage R&R study, movements during the scanning process caused serious issues and, in some cases, required rescanning of the surface. By making the enclosure of the device from a stiffer material and moving more weight closer to the bottom of the sensor should be able to reduce the movements during the scanning operation. Other important improvements would be to add a physical start button and place it so that it can be pushed while holding the sensor with both hands as well as reducing the time it takes from pushing the button until the scan is finished. In part, some of the movements may have been caused because it is difficult to keep the sensor still for a duration of five seconds. Hence a faster scanner would also be beneficial in this regard.

The results of the last two gage R&R studies are the most meaningful since similar surfaces are compared. In summary, the gage R&R results, which are lower than 10%, are great results since 10% is considered a cutoff value to determine if a measurement system is appropriate for a specific measurement task or not.

ACKNOWLEDGEMENT

This research is sponsored by the Defense Logistics Agency Information Operations, J68, Research & Development Office, Ft. Belvoir, Virginia and the DLA Troop Support, Philadelphia, Pennsylvania.

DISCLAIMER

REFERENCES

1. P. Eubanks, A. Crawford, L. Johnson, G. Larkin, W. Patschke, and E. Schoefer, "Standard for the Visual Inspection of Casting Surfaces," Manual, Des Plaines, Illinois, Steel Founders' Soc. Am. Alloy Cast. Inst. (1969).
2. MSS SP-55, "Quality Standard for Steel Castings for Valves, Flanges and Fittings and Other Piping Components--Visual Method for Evaluation of Surface Irregularities)," Manufacturers Standardization Society of the Valves & Fittings Industry (2016). https://msshq.org/page/SP55 (Link last accessed 01-23-2025.)
3. A802/A802M − 95 1982 (2015), "Standard Practice for Steel Castings, Surface Acceptance Standards, Visual Examination," ASTM Int. West Conshohocken, PA, pp. 3–5 (2015).
4. GAR C-9 Cast Microfinish Comparator surface roughness scale, Gar Electroforming (2019).
5. T.J. Schorn, *AFS Transactions,* 17–23, American Foundry Society (2006).
6. G. Daricilar and F. Peters, "Methodology for Assessing Measurement Error for Casting Surface Inspection," Int. J. Met. (2015). https://doi.org/10.1007/BF03355514 (Link last accessed 01-23-2025.)
7. F. Peters, R. Stone, K. Watts, P. Zhong, and A. Clemons, "Visual Inspection of Casting Surfaces," AFS Trans., vol. 121, p. 8 (2013).
8. D.-H. Lee and N.-G. Cho, "Assessment of surface profile data acquired by a stylus profilometer," Meas. Sci. Technol. (2012) https://doi.org/10.1088/0957-0233/23/10/105601 (Link last accessed 01-23-2025.)
9. X.D. Yang, J. C. Li, and T.B. Xie, "A Large Measuring Range Profilometer for Three-Dimensional Surface Topography Measurement," *Key Eng. Mater.* (2007). https://doi.org/10.4028/www.scientific.net/KEM.364-366.750 (Link last accessed 01-23-2025.)
10. H.T. Lancashire, "A simulated comparison between profile and areal surface parameters: *Ra* as an estimate of *Sa*," ArXiv (2017). http://arxiv.org/abs/1708.02284 (Link last accessed 01-23-2025.)
11. U.C. Nwaogu, N.S. Tiedje, and H.N. Hansen, J., "A non-contact 3D method to characterize the surface roughness of castings," Mater. Process. Technol. (2013).https://doi.org/10.1016/j.jmatprotec.2012.08.008 (Link last accessed 01-23-2025.)
12. M.M. Voelker and F.E. Peters, "Development of a digital standard to specify surface requirements of cast metal surfaces," *Mater. Perform. and characterization* (2008). https://doi.org/10.1520/MPC20160014 (Link last accessed 01-23-2025.)
13. D.M. Shivanna, M.B. Kiran, S.D. Kavitha, Procedia Mater. Sci., vol. 5, Elsevier (2014). https://doi.org/10.1016/j.mspro.014.07.416 (Link last accessed 01-23-2025.)
14. F. Darboux, P. Davy, C. Gascuel-Odoux, C. Huang, *CATENA,* (2002). https://doi.org/10.1016/S0341-8162(01)00162-X (Link last accessed 01-23-2025.)
15. E.C. Kamphorst et al., *Soil Sci Soc Am J*, 64, 1749–1758, (2000). https://doi.org/10.2136/sssaj2000.6451749x (Link last accessed 01-23-2025.)
16. T. Belem, F. Homand-Etienne, M. Souley, Rock Mech. Rock Eng. (2000).
17. R.B. Rusu and S. Cousins, "3D is here: Point Cloud Library (PCL)," in *2011 IEEE International Conference on Robotics and Automation* (May 2011) pp. 1–4, doi: 10.1109/ICRA.2011.5980567 (Link last accessed 01-23-2025.)
18. P. Alliez and A. Fabri, "CGAL: the computational geometry algorithms library," in *ACM SIGGRAPH 2016 Courses on - SIGGRAPH '16* (2016), pp. 1–8, doi: 10.1145/2897826.2927362 (Link last accessed 01-23-2025.)
19. J. Canny, "A Computational Approach to Edge Detection," *IEEE Trans. Pattern Anal. Mach. Intell.*, vol. PAMI-8, no. 6, pp. 679–698 (Nov. 1986). doi: 10.1109/TPAMI.1986.4767851 (Link last accessed 01-23-2025.)
20. "Point Cloud Library (PCL): pcl/features/organized_edge_detection.h Source File."https://pointclouds.org/documentation/organized__edge__detection_8h_source.html (Link last accessed 01-23-2025.)
21. D. Bazazian, J.R. Casas, and J. Ruiz-Hidalgo, "Fast and Robust Edge Extraction in Unorganized Point Clouds," *2015 Int. Conf. Digit. Image Comput. Tech. Appl. DICTA 2015*, 2015. doi: 10.1109/DICTA.2015.7371262 (Link last accessed 01-23-2025.)
22. H. Hoppe, T. DeRose, T. Duchamp, J. McDonald, and W. Stuetzle, "Surface reconstruction from unorganized points," *Comput. Graph.*, vol. 26, no. 2, pp. 71–78, 1992. doi: 10.1145/142920.134011 (Link last accessed 01-23-2025.)
23. D. Cohen-Steiner, F. Da, and F.A. Da, "A Greedy Delaunay Based Surface Reconstruction Algorithm." Accessed: Feb. 15, 2021. [Online]. Available: https://hal.inria.fr/inria-00072024 (Link last accessed 01-23-2025.)
24. M. Botsch and L. Kobbelt, "A Remeshing Approach to Multiresolution Modeling," (2004).
25. M. Botsch, L. Kobbelt, M. Pauly, P. Alliez, B. Lévy, *Polygon mesh processing*, CRC (2010).
26. FARO, FARO Edge and ScanArm ES, (FARO, 2013), ftp://ftp4.jgc.gr/Pdf_files/TechSheet_FARO Edge.pdf . (Link last accessed 06 Sep 2018.